Earthq Eng & Eng Vib (2008) 7:125-136 **DOI**: 10.1007/s11803-008-0832-9

Seismic vulnerability evaluation of axially loaded steel built-up laced members II: evaluations

Kangmin Lee[1†] and Michel Bruneau[2‡]

1. *Department of Architectural Engineering, Chungnam National University, Korea*
2. *Department of Civil, Structural, and Environmental Engineering, University at Buffalo, State University of New York, USA*

Abstract: The test results described in Part 1 of this paper (Lee and Bruneau, 2008) on twelve steel built-up laced members (BLMs) subjected to quasi-static loading are analyzed to provide better knowledge on their seismic behavior. Strength capacity of the BLM specimens is correlated with the strength predicted by the AISC LRFD Specifications. Assessments of hysteretic properties such as ductility capacity, energy dissipation capacity, and strength degradation after buckling of the specimen are performed. The compressive strength of BLMs is found to be relatively well predicted by the AISC LRFD Specifications. BLMs with smaller *kl/r* were ductile but failed to reach the target ductility of 3.0 before starting to fracture, while those with larger *kl/r* could meet the ductility demand in most cases. The normalized energy dissipation ratio, E_C/E_T and the normalized compressive strength degradation, C_r''/C_r of BLMs typically decrease as normalized displacements $\delta/\delta_{b,exp}$ increase, and the ratios for specimens with larger *kl/r* dropped more rapidly than for specimens with smaller *kl/r*; similar trends were observed for the monolithic braces. The BLMs with a smaller slenderness ratio, *kl/r*, and width-to-thickness ratio, *b/t*, experienced a larger number of inelastic cycles than those with larger ratios.

Keywords: seismic vulnerability; built-up compression member; strength capacity; ductility capacity; energy dissipation; strength degradation

1 Introduction

A companion paper (Lee and Bruneau, 2008) discussed a program of quasi-static testing of twelve steel built-up laced members (BLMs) through fracture. This series of tests provided useful data to evaluate and assess their hysteretic properties. BLMs are commonly used throughout the United States and are designed to resist wind forces, but not earthquakes.

The objective of this paper is to investigate and frame the experimentally observed data on cyclic behavior in terms that allow a quantitative assessment whether of BLMs can provide satisfactory seismic performance. Towards that end, the strength of the specimens obtained from testing is correlated with the predicted strength from the AISC LRFD Specification (1999), and the hysteretic response is quantified in terms of ductility capacity, energy dissipation capacity, and strength degradation after buckling of the specimen, and compared to seismic demands or comparable values for monolithic members.

Correspondence to: Kangmin Lee, Department of Architectural Engineering, Chungnam National University, Daejeon, 305-764, Korea
Tel: +82-42-821-5625; Fax: +82-42-823-9467
E-mail: leekm@cnu.ac.kr
†Assistant Professor; ‡Director, MCEER, Professor

Supported by: Federal Highway Administration Under Grant No. DTFH61-98-C-00094
Received February 27, 2008; **Accepted** April 21; 2008

2 Analysis of experimental results

2.1 Compression strength

Buckling strengths of specimens were calculated per the AISC LRFD Specification considering the various limit states of the global flexural buckling, local buckling, and buckling of the built-up member due to shearing effect.

Flexural buckling equations for compression members are specified by AISC LRFD as:

For $\lambda_c = \frac{kl}{r\pi}\sqrt{\frac{F_y}{E}} \le 1.5$

$$P_n = A_g F_{cr} = A_g (0.658^{\lambda_c^2}) F_y \quad (1a)$$

For $\lambda_c = \frac{kl}{r\pi}\sqrt{\frac{F_y}{E}} > 1.5$

$$P_n = A_g F_{cr} = A_g \left[\frac{0.877}{\lambda_c^2}\right] F_y \quad (1b)$$

Axially loaded members containing elements subjected to compression with a width-thickness ratio, *b/t*, in excess of the AISC LRFD limitations are designed as follows:

For $\lambda_c\sqrt{Q} \le 1.5$,

$$P_n = A_g F_{cr} = A_g Q(0.658^{Q\lambda_c^2})F_y \tag{2a}$$

For $\lambda_c\sqrt{Q} > 1.5$

$$P_n = A_g F_{cr} = A_g\left[\frac{0.877}{\lambda_c^2}\right]F_y \tag{2b}$$

where Q is the reduction factor for slender compression elements.

For built-up compression members, for intermediate connectors that are snug-tight bolted, $(kl/r)_m$ is given by:

$$\left(\frac{kl}{r}\right)_m = \sqrt{\left(\frac{kl}{r}\right)_0^2 + \left(\frac{a}{r_i}\right)^2} \tag{3a}$$

and for intermediate connectors that are welded or fully-tensioned bolted.

$$\left(\frac{kl}{r}\right)_m = \sqrt{\left(\frac{kl}{r}\right)_0^2 + 0.82\frac{\alpha^2}{(1+\alpha^2)}\left(\frac{a}{r_{ib}}\right)^2} \tag{3b}$$

In comparing the experimental results with theoretical values, it is important to use a value of *k* representative of the actual system tested. This estimate is done differently for the specimens with slenderness ratios of 60 and 120.

As would be the case for an actual braced bent, the specimens with *kl/r* of 60 are subjected to a bending moment and are not in pure compression when the frame sways. Therefore, inflection points can be determined along the braces and the distance, *l** is defined as the distance between two inflection points. The actual *k* factor for the specimens is therefore given by the ratio of *l*/l*, where *l* is the distance between the first row of bolts at the face of the gusset to the same on the other gusset. SAP 2000 analyses results show that the effective length factor, *k*, for the tested specimens varies between 0.61 to 0.68 with an average value of 0.65.

The compression strength for the specimens named *kl/r* = 60 calculated per the equations of AISC LRFD design specification with consideration of the specific buckling modes of each specimen and using the effective member length factor obtain from these SAP 2000 analyses are then compared with the test results as shown in Fig. 1. Note that the deviation of the calculated specimen strengths from the experimental values is within 20 percents except for specimen By8-60. This greater error of specimen By 8-60 could be attributed to an initial imperfection introduced at the beginning of the test of the specimen. Elastic buckling strength of compression members having initial imperfection, *a*, is obtained as (Gere and Timoshenko, 1984):

$$b_1\left(\frac{P}{A_g}\right)^2 - b_2\left(\frac{P}{A_g}\right) + \sigma_{max} = 0 \tag{4}$$

where $b_1 = \frac{1}{\pi^2 E}\left(\frac{l}{r}\right)^2$, $b_2 = 1 + \frac{ac}{r^2} + \frac{\sigma_{max}}{\pi^2 E}\left(\frac{l}{r}\right)^2$, $\frac{ac}{r^2}$ is the imperfection ratio, *a* is the maximum initial imperfection, and *c* is distance from the centroidal axis to the extreme fiber on the concave side of the compressive member.

The member initial imperfection to length ratio, *a* is approximately 1/300. As a result, the compressive strength of the By8-60 specimen was recalculated per Eq. (4), and the modified calculated strength deviation of the specimen is about 10% as shown in Fig. 1.

For the specimens with *kl/r* = 120, the effective length factors, *k* predicted by the AISC LRFD Specification, theoretically, are 1.0 (AISC, 1999). From the bending moment diagrams obtained from SAP 2000 analyses, these factors are slightly larger than 1.0. However, in the first step, the expected design compressive strength of these specimens was calculated here with *k* = 1.0. Resulting calculated values are compared with those obtained from testing in Fig. 2. Note that the AISC LRFD Specification equations underestimate the compressive strength of the test specimens with a slenderness ratio of 120 with a relatively large error (from 12% to 45%).

To make the calculated strength equal to the tested value, the effective length factor, *k* values for the specimens with *kl/r* of 120 should be varied from 0.76 to 0.93 (the average being 0.83).

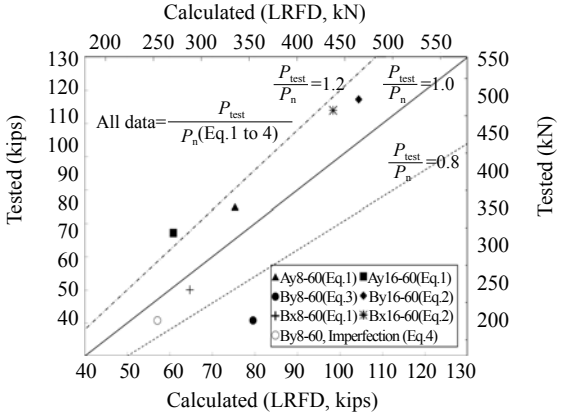

Fig. 1 Compressive strength comparisons (*kl/r* = 60)

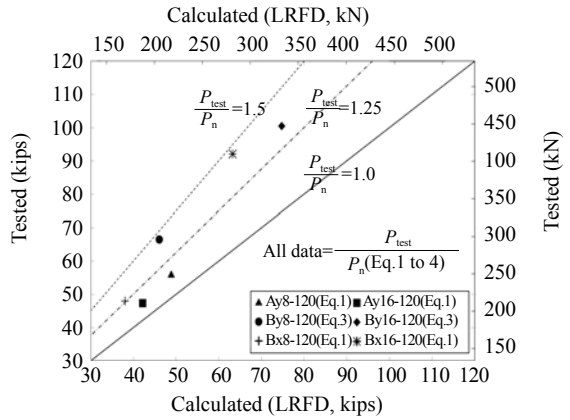

Fig. 2 Compressive strength comparisons (*kl/r* = 120)

2.2 Ductility capacity

To compare the relative hysteretic behavior of test specimens with different slenderness ratios and width-to-thickness ratios but the same cross-section type (i.e. Ay, By, and Bx), normalized hysteretic curves are illustrated in Figs. 3 to 5, respectively. In the figures the normalized displacement represents the tested displacement to the tested buckling displacement ($\delta_{b,exp}$), and the normalized force represents the tested force to the theoretical yield force of the test specimen calculated as $P_y = A_g\sigma_y$.

To assess the adequacy of the hysteretic behavior of the braces, capacity must be compared against demand. One way to quantify demand is in terms of displacement demands, themselves related to the design level, and the structural response modification, R, defined as the product of the ductility factor (R_d) and the over-strength factor (Ω_0) of a structural system. For braced frames, the design (or evaluation) assumption also has an impact on demand. For example, for a given ductility reduction factor, R_d, a tension-only braced frame would be designed to resist the entire base shear V equal to the forces obtained from the elastic response spectrum divided by R_d. Consequently, in that case, the brace force is calculated dividing V by the cosine angle of the brace as shown in Fig. 6. Alternatively (and more conventionally), each brace force in a standard X-braced frame can be determined by dividing $V/2$ by the cosine angle of the brace as shown in Fig. 7. In such a case, compression strength of the brace governs the design.

In the AISC LRFD Specification, the ductility factor for braced frames is assumed to be 3. The over-strength factor specified for CBF is 2 and R factor is 6, corresponding to a ductility factor of 3. This value is shown in Figs. 3 to 5 by thick vertical dotted lines which can be used to assess whether the ductility capacity of specimens is sufficient to meet the specified demands. As schematically presented in Fig. 7, ductility

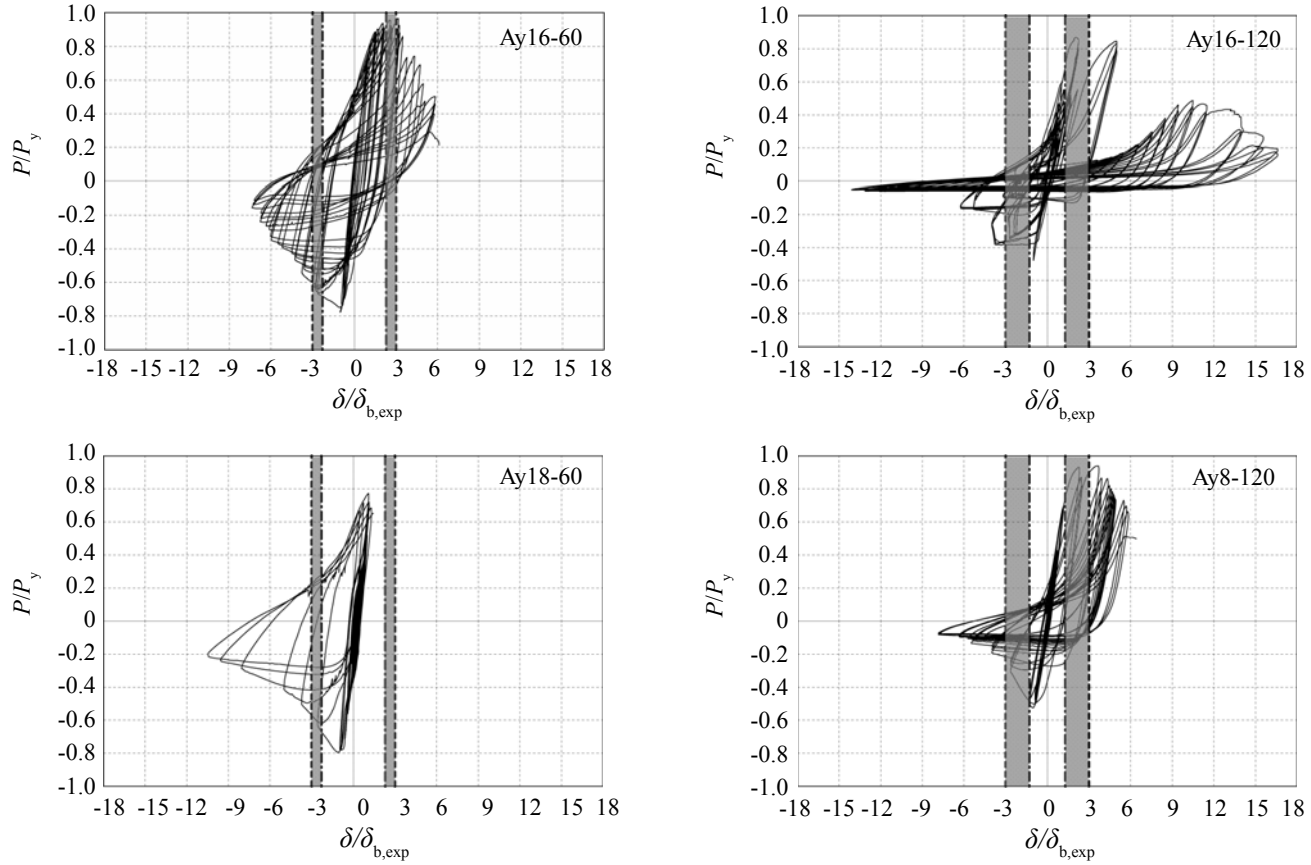

Fig. 3 Normalized hysteretic curves for specimens Ay

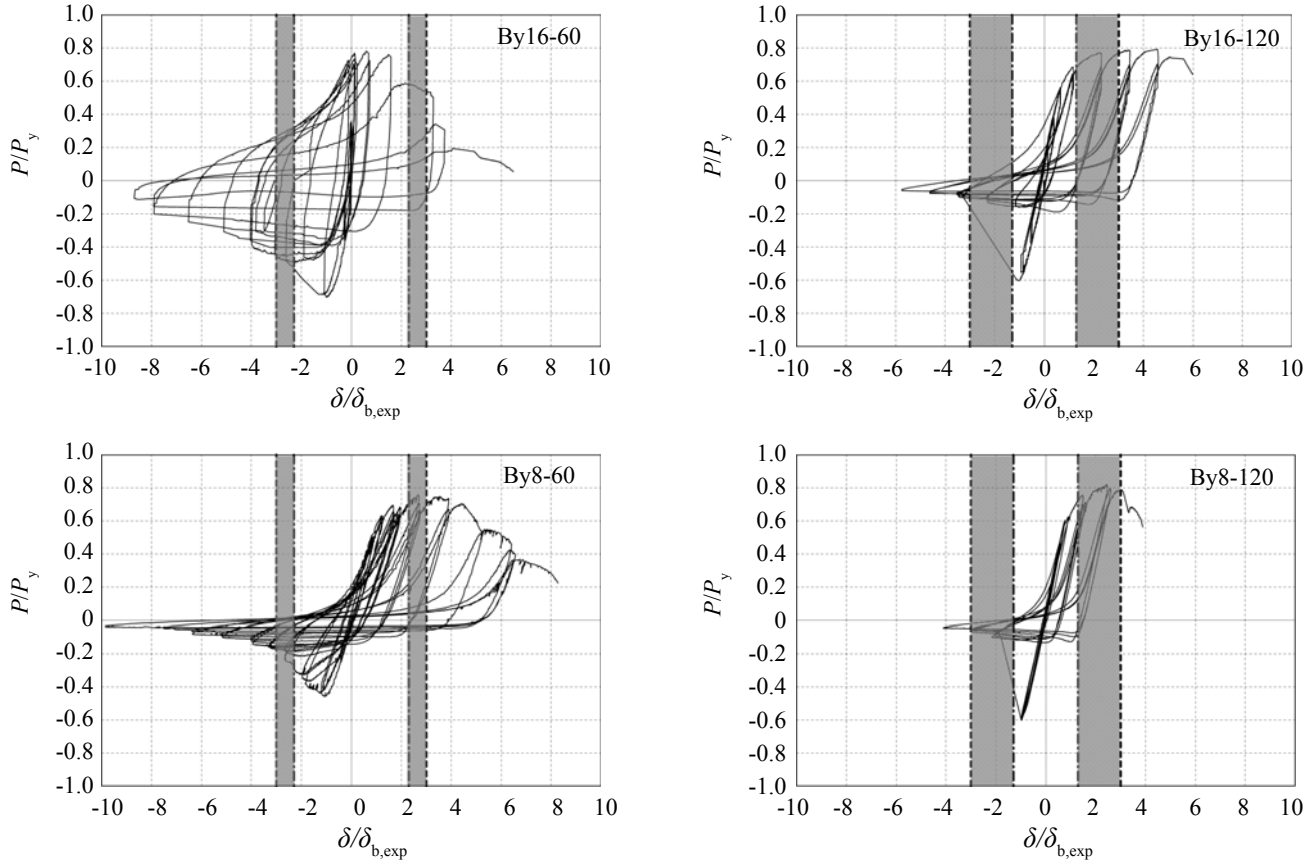

Fig. 4 Normalized hysteretic curves for specimens By

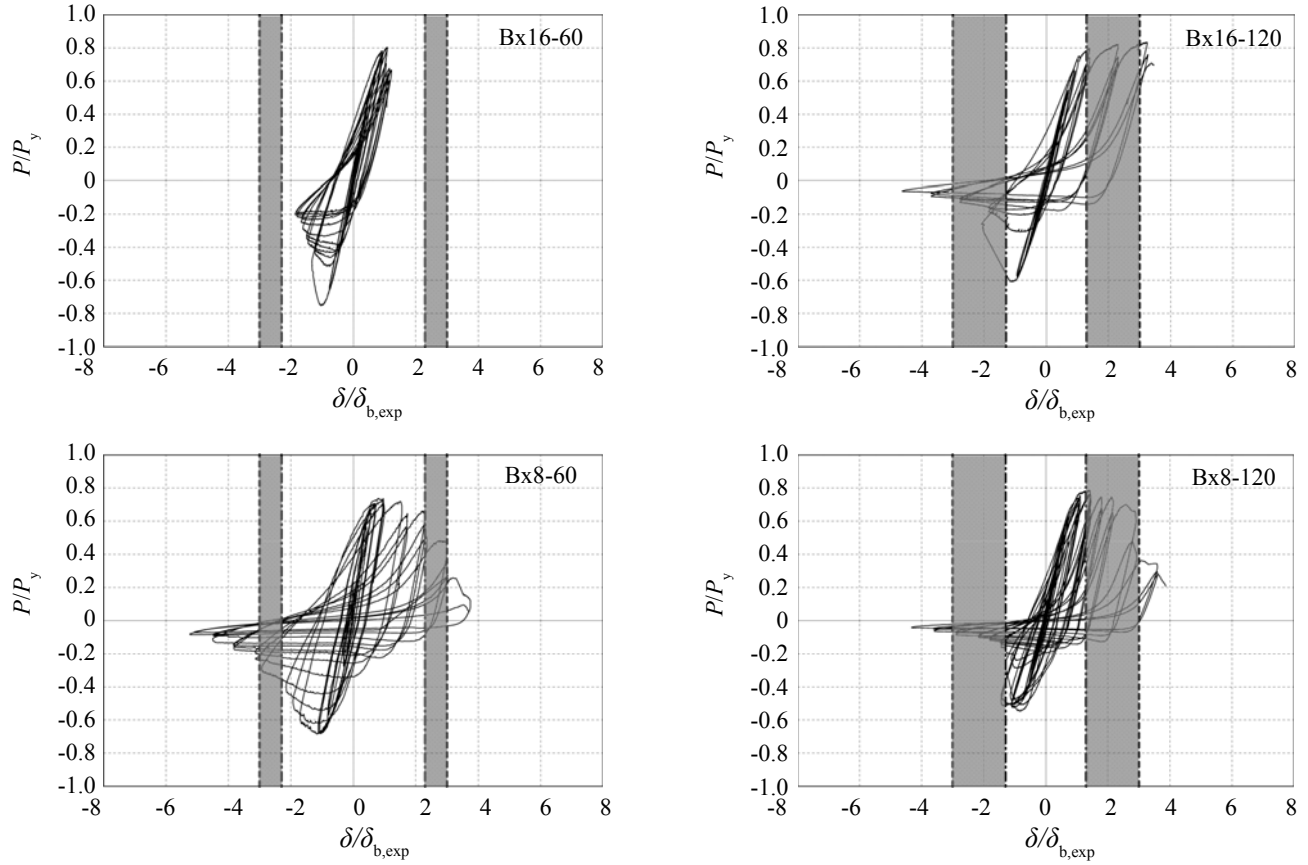

Fig. 5 Normalized hysteretic curves for specimens Bx

capacity of the bracing members in a X-braced frame is calculated as:

for a compressive bracing member,

$$\mu_b = \frac{\delta_{max}}{\delta_b} \tag{5a}$$

and for a tensile bracing member,

$$\mu_y = \frac{\delta_{max}}{\delta_y} \tag{5b}$$

The relationship between compressive and tensile ductility capacities is a function of the slenderness ratio, *kl/r* of the bracing member. If an X-braced frame has slender bracing members, a smaller tensile ductility demand will be required compared to an X-braced frame with stockier bracing members as schematically presented in Fig. 8. An example calculation of tensile ductility, μ_y corresponding to the compressive ductility, μ_b of 3 for compressive members with slenderness ratios of 60 and 120 is schematically presented in Fig. 9. In this figure, design stress for compression members with *kl/r* of 60 and 120 were taken from the AISC LRFD Specification design stress table for Gr. 345 MPa steel. These values were divided by the design stress for a compression member with *kl/r* = 0, which corresponds to the tensile stress of the member. Consequently, these ratios can be translated into the ratio of compressive buckling displacement to tensile yield displacement (δ_b /δ_y) of the bracing members. The corresponding relationships $\delta_b = 0.77\delta_y$ and $\delta_b = 0.35\delta_y$ are obtained for bracing members with slenderness ratios of 60 and 120, respectively, from which respective tensile ductility of 2.3 and 1.1 (corresponding to δ_b of 3) are calculated. These values are also presented by thick vertical dash-dotted lines in the normalized hysteretic curves of Fig. 3 to 5. The area enclosed within the shaded areas illustrate the expected range of ductility demands for these members per the above. Ductility capacities obtained from the testing of specimens are also presented in Table 1.

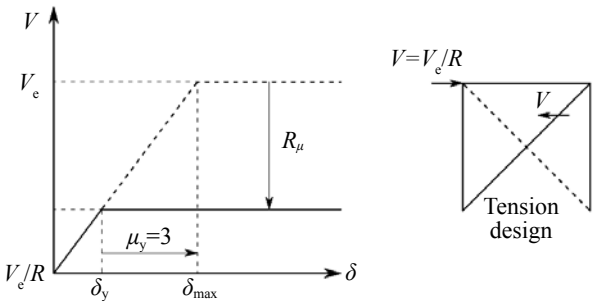

Fig. 6 Tension only braced frame design

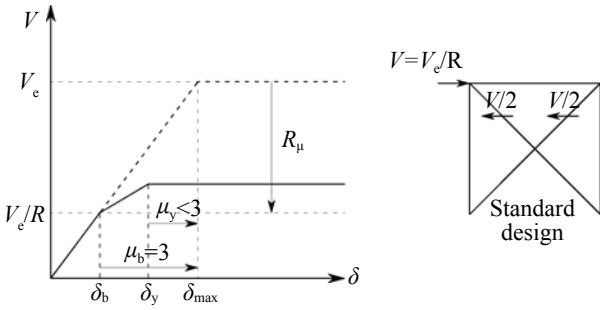

Fig. 7 X-braced frame design

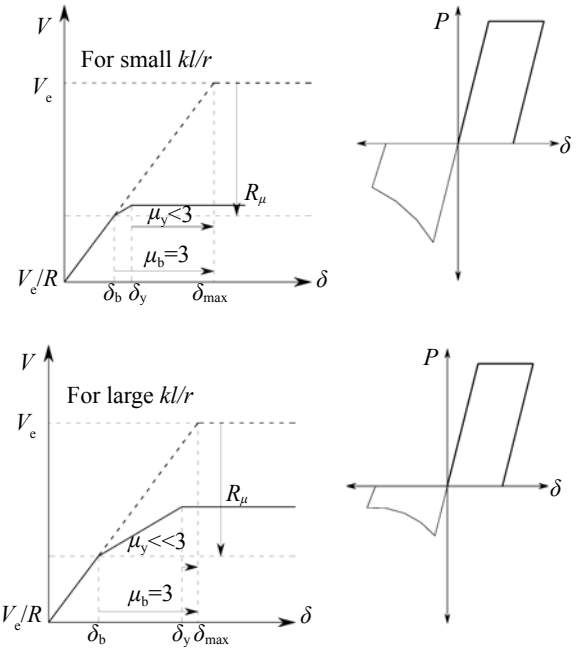

Fig. 8 Ductility comparisons between slender and stocky braces in a X-braced frame

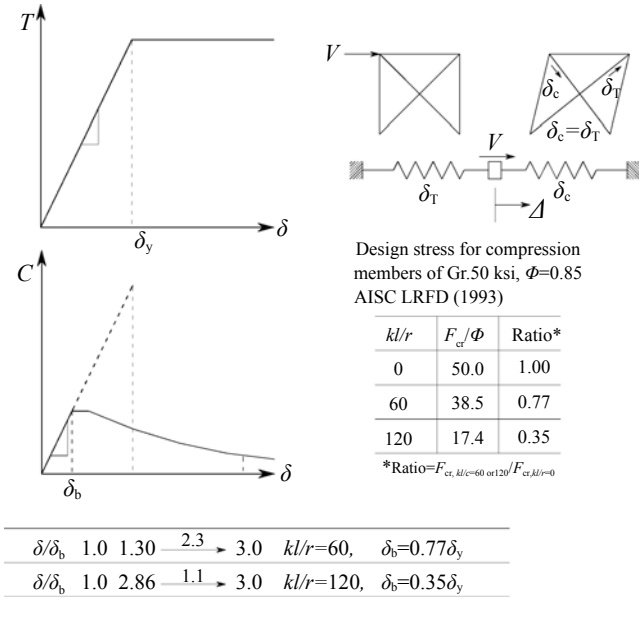

Fig. 9 Relationship between compressive and tensile ductility

Table 1 Ductility capacity comparisons

Specimen	μ_b	μ_y	μ_y^{*1}	Specimen	μ_b	μ_y	μ_y^{*1}
Ay16-60	4.60	4.69	2.67	Ay16-120	14.09	16.99	5.00
Ay8-60	6.89	N/A*2	N/A*2	Ay8-120	7.85	9.51	3.72
By16-60	5.48	7.33	3.71	By16-120	5.74	8.83	5.68
By8-60	8.26	8.60	4.67	By8-120	4.12	5.11	3.09
Bx16-60	2.29	2.77	2.29	Bx16-120	4.63	4.71	3.23
Bx8-60	3.71	3.63	2.56	Bx8-120	4.32	3.86	2.89

*1. The observed ductility before relatively large strength degradation in tension after initial fracture.
*2. Specimen Ay8-60 did not reach its maximum tensile strength.

Note that the term δ_y^* is used to quantify the tensile ductility reached before a significant drop in tensile strength occurs due to initial fracture.

The specimens with section shape "A" and *kl/r* of 120 had a sufficient ductility to meet the ductility demand of 3.0. The specimen Ay16-60 barely met the target ductility demand of 3.0 and upon initial fracture of the specimen at experimentally obtained ductility of 2.67, tensile strength dropped rapidly. Finally, results for specimen Ay8-60 are inconclusive because it was not tested in tension for reasons explained earlier.

Specimens with section shape "By" all exhibited satisfactory ductility capacity and met the target ductility demand of 3.0. Specimens By16-120 and By8-60 reached the largest ductility capacity in tension although the drop in tension strength was more sudden for specimen By16-120 than for specimen By8-60. The other two specimens exhibited development and progression of fracture almost immediately after the target ductility was reached.

Specimens with section shape "Bx" exhibited the worst cyclic inelastic performance, where all specimens failed to reach the target ductility of 3.0 before starting to fracture with the exception of the Bx16-120 specimen which fractured just after reaching the target ductility of 3.0. Specimen Bx16-60 had the worst behavior among all specimens in this category as it started to develop fracture at ductility less than 2.0.

Specimens with both larger slenderness and width-to-thickness ratio showed the best ductility performance while the specimens with smaller slenderness and larger width-to-thickness ratio showed the worst ductility capacity. For the specimens with slenderness ratio, *kl/r* of 60, those with larger width-to-thickness ratios, *b/t*, showed lower ductility capacity than those designed with smaller *b/t*, because local buckling precipitated low cycle fatigue. However, comparing the ductility of the specimens with *kl/r* of 120, it appears that ductility capacity of the slender specimens was not greatly affected by the *b/t* ratios. Note that initial global buckling was observed during the testing of the specimens with *kl/r* of 120, irrespectively of their *b/t* ratios. Additionally, specimens with section shape "A" exhibited the most ductile behavior, and specimens with section shape "Bx" the worst.

When compared with monolithic braces (Lee and Bruneau, 2002), built-up braces with larger *kl/r* were shown to have less ductility capacity, while those with smaller slenderness ratio showed ductility capacity comparable to monolithic bracing members.

2.3 Energy dissipation capacity

To assess the energy dissipation capacity of compressive BLMs, the energy dissipated during testing by each specimen was calculated from the experimentally obtained hysteretic force-axial deformation curves of the specimens. The tension and compression energy dissipation was calculated for each cycle as a product of the compression or tension force times the axial deformation. The normalized energy, $E_C/E_{C,cal}$ or $E_T/E_{T,cal}$, where E_C and E_T, respectively, represent the calculated energy dissipation in compression and tension obtained from testing, and $E_{C,cal}$ and $E_{T,cal}$ denote the theoretically compressive and tensile energy that would have been dissipated by the member in compression/tension if the same maximum axial displacement was reached during unloading of the member after its elongation as schematically shown in Fig. 10 (Lee and Bruneau, 2002; 2005). Note that the notation $E_{T,cal}$ is identical with E_T used by Lee and Bruneau (2002) to differentiate with the calculated energy dissipation in tension obtained from testing. Note that the axial deformation in compression, δ, is measured from the point of zero member force (which may not correspond to the original zero displacement position) up to the point of maximum compressive deformation, as illustrated in Fig. 10, as δ_c. Normalized energy ratio of each cycle of the specimens was then accumulated until the entire fracture of the specimens and results are shown in Table 2. The average values of normalized cumulative energy dissipation capacity for monolithic braces of various cross sections reported by Lee and Bruneau (2002, 2005) are also presented in term of their *kl/r* ranges for comparison purposes.

The specimens "Ay" and "By" with *b/t* ratio of 16 experienced more inelastic cycles and deformation, consequently dissipated more cumulative compressive energy than the specimens with *b/t* ratio of 8. For the "Ay" and "By" specimens with *kl/r* of 60, comparisons of the cumulative energy ratios between specimens with

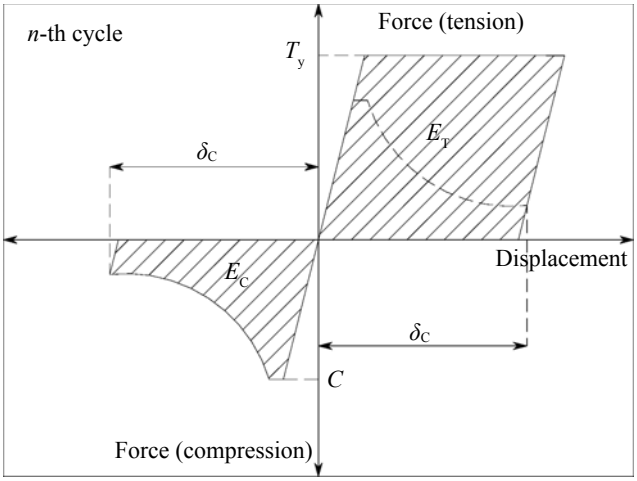

Fig. 10 Definition of dissipated energy ratio, E_C / E_T (Lee and Bruneau, 2002)

b/t ratios of 8 and 16 is not possible, because testing of the specimens Ay8-60 stopped before fracture, and specimen By8-60 would have been able to dissipate more normalized energy ratio during their first few cycles after buckling if not for this initial imperfection. Additionally, for specimens "Bx" with *kl/r* of 60, the difference of the cumulative energy ratios between Bx8-60 (*b/t* = 8) and Bx16-60 (*b/t*=16) was relatively small, approximately within 10 percent, and consequently no general trend is observed in their cumulative energy ratios.

Built-up braces with larger *kl/r* were able to dissipate more normalized energy than those with smaller *kl/r*, which is similar to the trend observed for monolithic braces (Lee and Bruneau, 2002; 2005). On average, the BLM specimens with section shape "B" dissipated less normalized cumulative energy than monolithic bracing members; however those with section shape "A"

Table 2 Normalized cumulative energy in compressions, $\Sigma(E_C/E_T)$

Built-up braces								
b/t	*kl/r* = 60				*kl/r* = 120			
8	Ay8-60 = 3.06*				Ay8-120 = 4.02			
	By8-60 = 2.71		Avg. = 3.25		By8-120 = 1.19		Avg. = 3.17	
	Bx8-60 = 3.97				Bx8-120 = 4.31			
16	Ay16-60 = 7.61				Ay16-120 = 4.52			
	By16-60 = 4.78		Avg. = 5.29		By16-120 = 1.38		Avg. = 2.59	
	Bx16-60 = 3.47				Bx16-120 = 1.86			
Monolithic braces								
kl/r	Average	WF	Tube	Pipe	DA	WT	Angle	DC
0-75	3.66	3.44	2.50	4.71	3.25	N/A	N/A	N/A
75-125	1.98	2.04	1.88	3.73	1.68	2.82	0.42	1.86
125-200	1.23	N/A	N/A	N/A	1.23	N/A	N/A	N/A

* Specimen Ay8-60 did not reach its entire fracture

dissipated slightly more normalized cumulative energy.

2.4 Strength degradation

Strength degradation of the compression member after buckling depends on their slenderness ratios and width-to-thickness ratios. To quantify the strength degradation of the built-up laced compression specimens upon repeated cycling loads, test results were processed following the same procedures as schematically shown in Fig. 11, which were used by Lee and Bruneau (2002, 2005). The strength degradation of the specimens in compression, C_r''/C_r, was obtained at the various levels of normalized deformations (using the experimentally obtained buckling displacement, $\delta_{b,exp}$) for each specimen as shown in Figs. 12 to 14.

Note that the normalized compressive strength degradation, C_r''/C_r, of the specimens with *kl/r* of

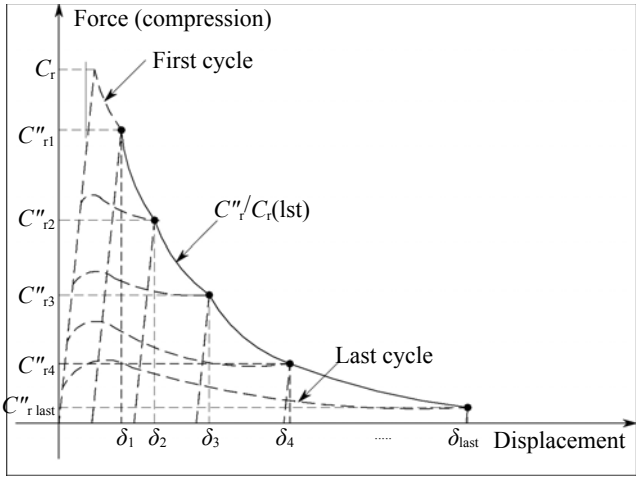

Fig. 11 Definition of normalized buckling capacity, C_r''/C_r (Lee and Bruneau, 2002)

120 was more severe than specimens with *kl/r* of 60. Lacing buckling in BLMs greatly affects the strength degradation because as the components of a brace move closer together, the moment of inertia of the section at that location is reduced. The plastic moment at these hinges is also reduced, and thus the loss in compression strength is accelerated. At a normalized displacement, $\delta/\delta_{b,exp}$, of 5, the normalized compressive strength of specimens with *kl/r* of 120 drops 50 to 60 percent of the maximum value for the section shape "A" specimens and 70 to 80 percent for the section shape "B" specimens. For section shape "A" and "B" specimens having slenderness ratio of 60, the corresponding reductions are 30 to 40 percent, and 50 to 70 percent in most cases. Additionally, slopes of the degradation, from the initial buckling to the normalized displacement, $\delta/\delta_{b,exp}$, of 5, were steeper for the specimens with *kl/r* of 120. This is a similar trend to what was observed for monolithic braces by Lee and Bruneau (2002).

2.5 Low cycle fatigue fracture life

Another factor that impacts the behavior of compression members is fracture upon low cycle fatigue under repeated cyclic loading. Upon repeated cyclic loading, the local buckling and straightening of the material at that location induce cracks that may propagate and lead to fracture. Two different fracture criteria of tubular bracing members are reviewed in this section.

Tang and Goel (1987) introduced an empirical fracture criterion for rectangular tubular bracing members. This criterion requires a special calculation of the number of cycles that contribute to fatigue life. To count these cycles, Tang and Goel established the rules applicable to a brace axial deformation time history (refer to Fig. 15). Lee and Goel (1987) reformulated this model by considering the effect of F_y and eliminating the dependency on *kl/r*. In this criterion, the theoretical fracture life, Δ_f is expressed as follows:

$$\Delta_f = C_s \frac{(46/F_y)^{1.2}}{[(B-2t)/t]^{1.6}}\left(\frac{4B/D+1}{5}\right) \tag{6}$$

where C_s is an empirically obtained constant calibrated from test results, and is the yield strength of the brace. Fracture is assumed to occur when $\Delta_{f,exp} = \Delta_f$.

Archambault *et al.* (1995) presented another criterion, in which the effect of slenderness ratio, *kl/r*, was re-introduced. Based on a review of previous test results, they found that the model proposed by Tang and Goel (1987) underestimates the fracture life of tubular bracing members with large slenderness ratios. Two distinct trends were noted for fracture life of bracing members as a function of *kl/r*, depending on whether slenderness was lower or higher than 70. They introduced the term, Δ_f^* (to differentiate it from Δ_f used by Tang and Goel), and expressed fatigue life as follows:

$$\Delta_f^* = C_s \frac{(317/F_y)^{1.2}}{[(B-2t)/t]^{0.5}}\left(\frac{4B/D+1}{5}\right)^{0.8} \times (70)^2 \text{ for } kl/r < 70 \tag{7a}$$

$$\Delta_f^* = C_s \frac{(317/F_y)^{1.2}}{[(B-2t)/t]^{0.5}}\left(\frac{4B/D+1}{5}\right)^{0.8} \times (kl/r)^2 \text{ for } kl/r \geq 70 \tag{7b}$$

To quantitatively access the low cycle fracture life of the built-up specimens, the experimental fracture life, $\Delta_{f,exp}$, of test specimens was calculated following the Tang and Goel (1987) method (also used by Archambault *et al.*, 1995). The experimental fracture life of bracing member was calculated from the axial force-displacement hysteretic curve normalized by tensile yield force, P_y and yield displacement, δ_y respectively.

Using proposed equations of the fracture life of bracing members by Tang and Goel (1987, Eq. (6)) and Archambault *et al.* (1995, Eq. (7)), fracture life of test specimens was calculated, then compared with those obtained from experimental results as shown in Table 3 and Fig. 16. Note that contrary to Tang and Goel's model, Archambault's *et al.* model overestimated the fracture life. As described earlier, these fracture criteria were developed to predict the fracture life of tubular bracing members, and it is therefore not surprising that they do not provide accurate estimates of the fracture life of built-up brace specimens. To this end, a new model applicable for the built-up bracing members is proposed, and is calibrated using the experimental data obtained in this study.

Figure 16 shows that Archambault's *et al.* model underestimated the experimental fracture life of the built-up specimens for 8 out of 11 specimens (recall that the twelfth specimen is Ay8-60 for which testing was stopped before fracture), with an average experimental to predicted fracture life ratio of 1.12 and a standard deviation of 1.03. Conservatively, Tang and Goel's model overestimated the experimentally obtained fracture life for 7 out of 11 specimens, with an average ratio of 2.24 and a standard deviation of 2.19. The new model proposed for the built-up bracing members needed to be calibrated to be between these two models, i.e., safer than Archambault's model and less conservative than Tang and Goel's mode. As described above, Archambault's model more closely predicted the fracture life of the specimens than Tang and Goel's model, and development of the new model was therefore based on Archambault's *et al.* model (e.g., Eq. (7)). Archambault's *et al.* model mainly differs from Tang and Goel's model in that it considers the impact of the slenderness ratio of the bracing member on fracture life. However, for the built-up brace specimens in this study, the slenderness ratio was not found to be have an impact on fracture life and its effect is therefore ignored in the

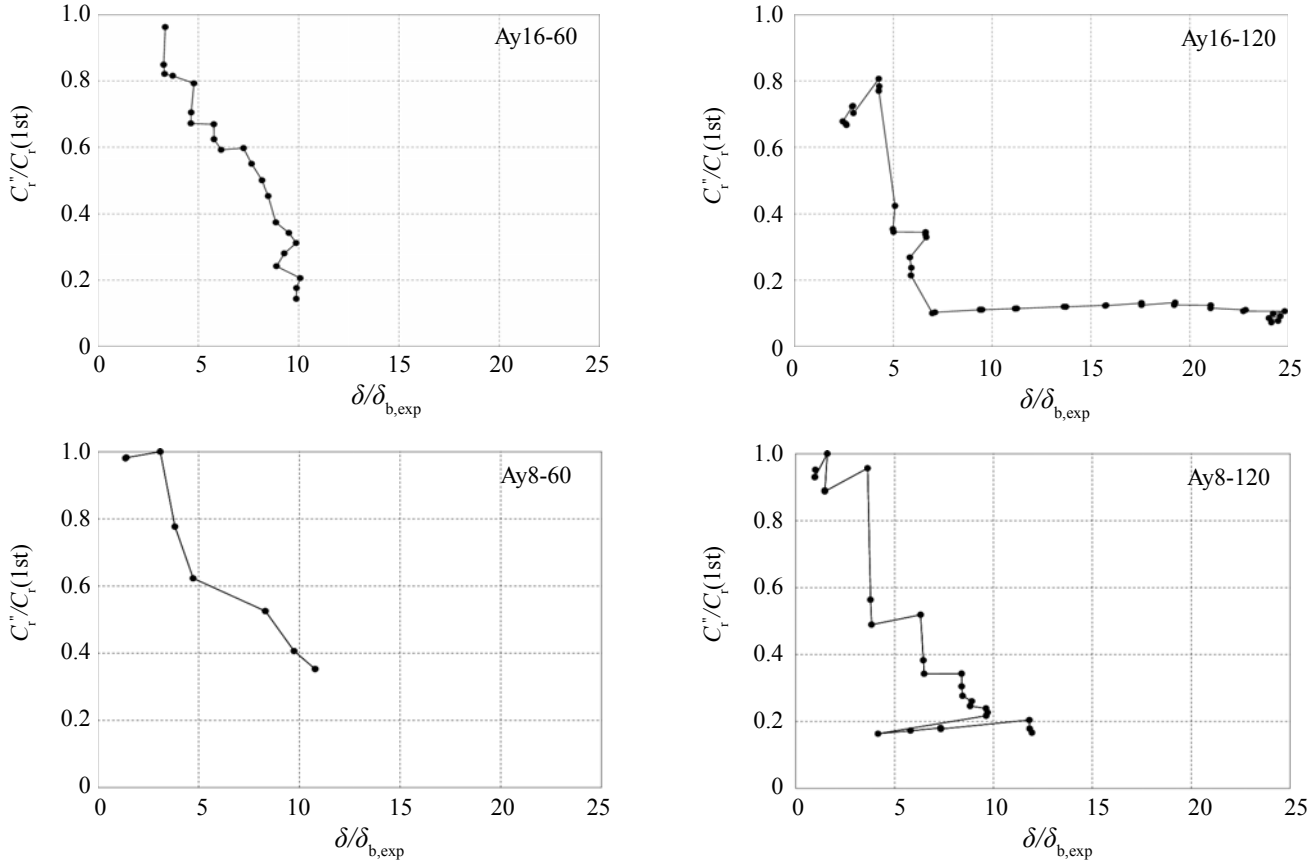

Fig. 12 Normalized buckling capacity, C_r'' / C_r for specimens Ay

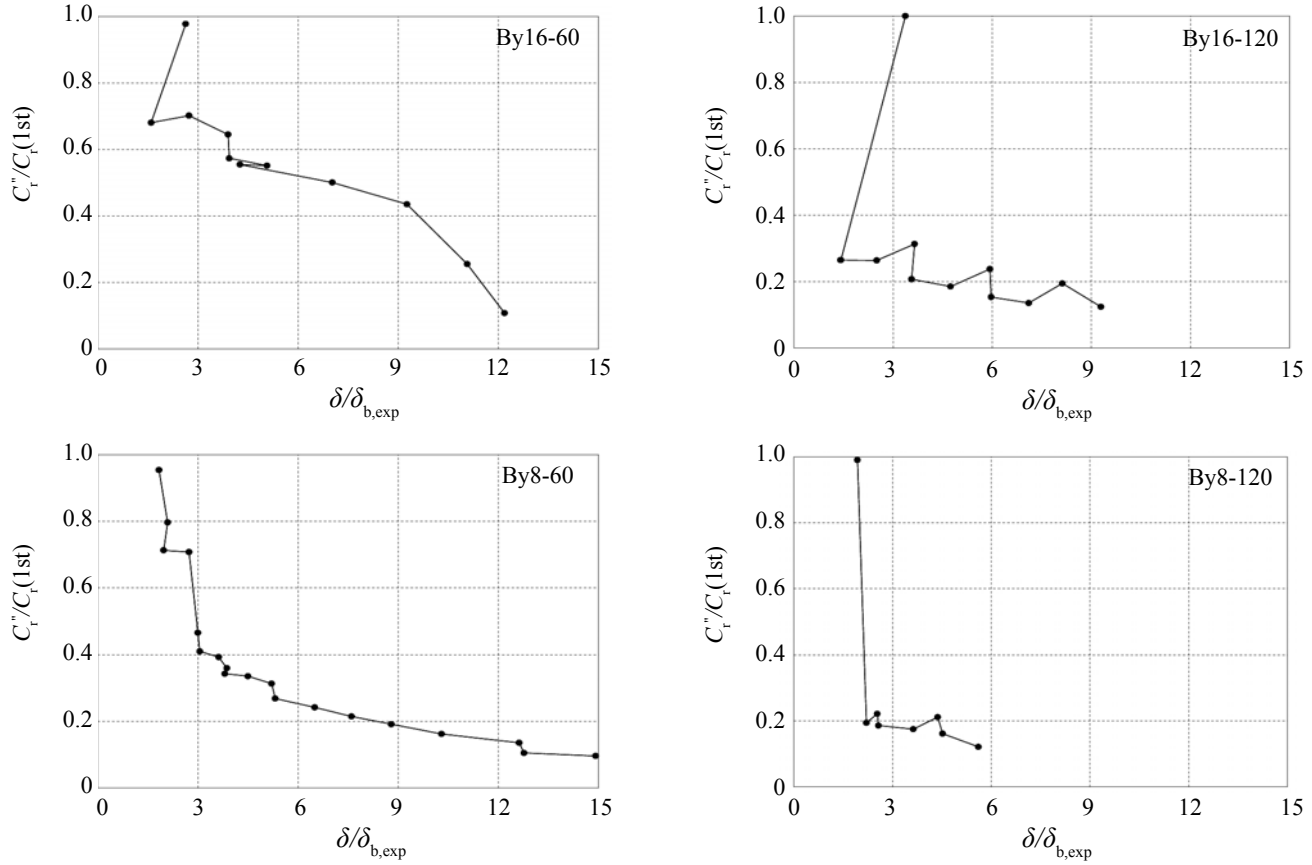

Fig. 13 Normalized buckling capacity, C_r'' / C_r for specimens By

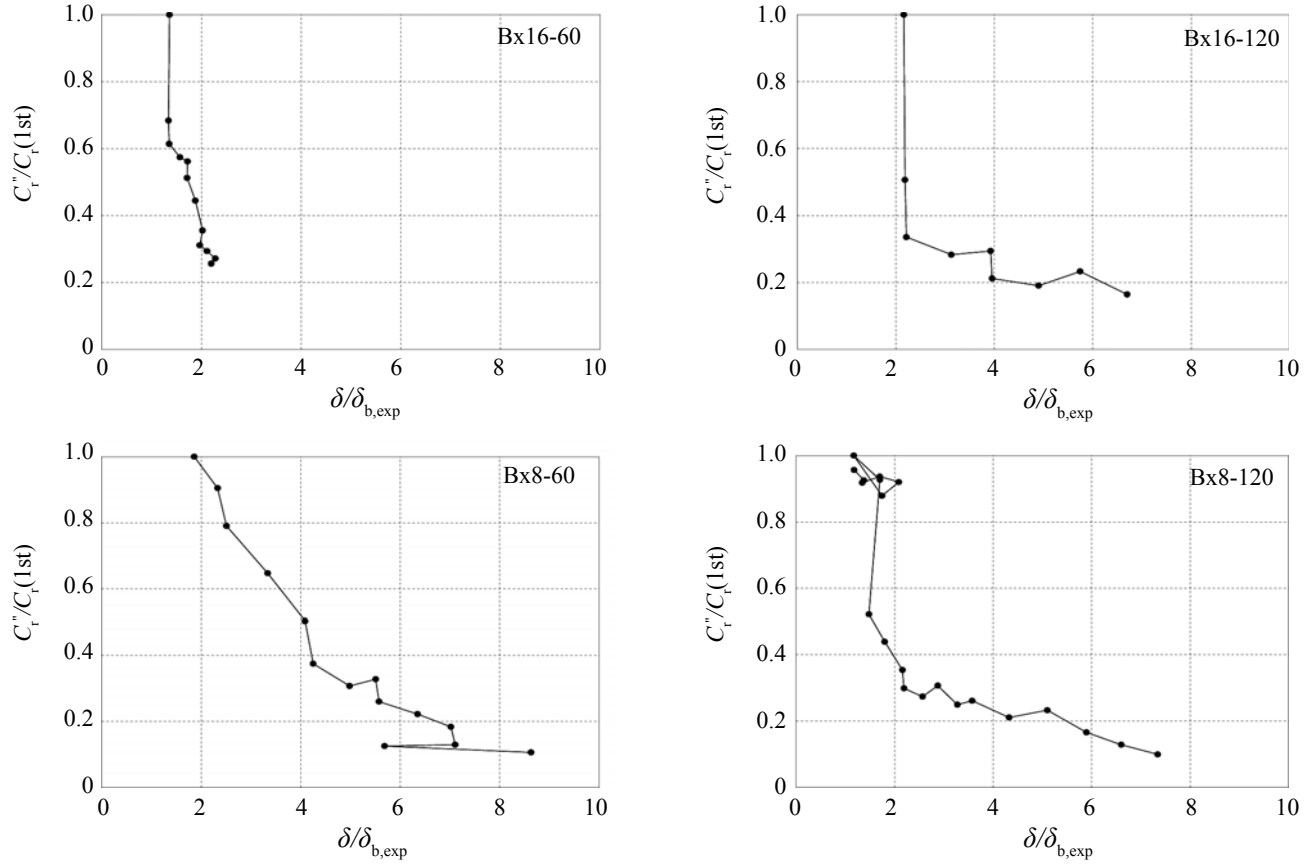

Fig. 14 Normalized buckling capacity, C_r'' / C_r for specimens Bx

new model. Additionally the shape factor term, [(4*B*/*D*+1)/5], was again removed for consistency because it considers the width-to-depth ratio of tubular bracing member on the fracture life, which is not applicable for built-up braces. As a result, Eq. (7) was simplified to:

$$\Delta_f^{**} = C_s \frac{(46/F_y)^{1.2}}{(b/t)^{0.5}} \tag{8}$$

The effect of yield stress (i.e., the term $(46/F_y)^{1.2}$ in Eq. (8)) was not changed for lack of better data. Then, best values for the numerical coefficient term, C_s, and exponent to the width-to-thickness term, $(b/t)^{0.5}$, were sought to find the equation that best predicted the fracture life of built-up brace members. The resulting equation was found to be:

$$\Delta_f^{**} = C_s \frac{(46/F_y)^{1.2}}{[b/t]^{0.7}} \tag{9}$$

where the numerical coefficient is 155.

Using Eq. (9), results for the test specimens are also presented in Fig. 16. Note that the fracture life of the built-up bracing member thus obtained are safer than predicted by Archambault's *et al*. model and less conservative than Tang and Goel's model, with an average ratio of experimental to predicted fracture life of 1.78 and a standard deviation of 1.38.

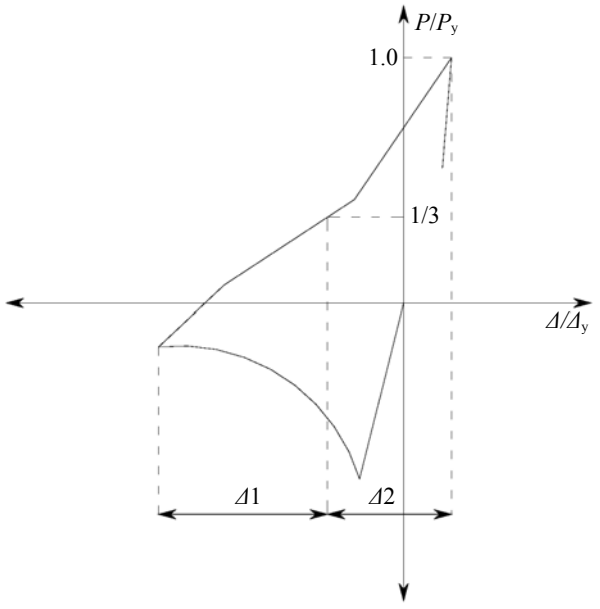

Fig. 15 Definition of $\Delta 1$ and $\Delta 2$ (Tang and Goel model, 1987)

Table 3 Predicted fracture life the specimens (Δ_f and Δ_f^*)

Specimen	Δ_f	Δ_f^*	Specimen	Δ_f	Δ_f^*
Ay16-60	14.8	24.4	Ay16-120	14.8	51.0
Ay8-60	37.9	28.7	Ay8-120	37.9	52.7
By16-60	18.1	28.7	By16-120	18.1	32.5
By8-60	59.3	40.7	By8-120	59.3	59.0
Bx16-60	12.8	21.8	Bx16-120	12.8	31.1
Bx8-60	43.5	31.7	Bx8-120	43.5	54.7

Δ_f: Tang and Goel (1987); Δ_f^*: Archambault *et al*. (1995)

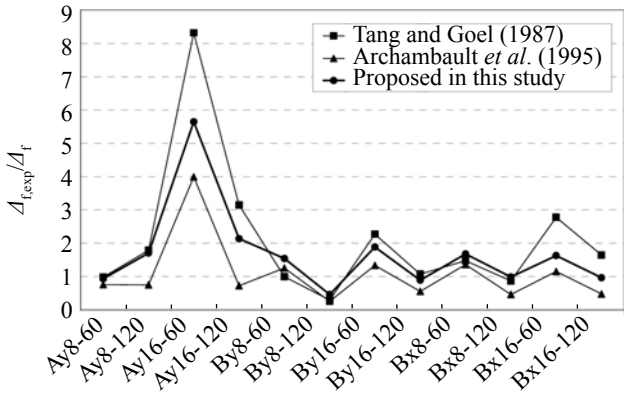

Fig. 16 Comparisons of fracture life of the specimens

3 Conclusions

Data was gathered in a previously described experimental test program of steel built-up laced member (BLM) specimens subjected to quasi-static loadings up to fracture (Lee and Bruneau 2004). From the analyses of experimental data of twelve BLMs, and comparisons to seismic demands or comparable values for monolithic braces, the following conclusions are made.

The BLMs with both larger *kl/r* and *b/t* showed best ductility performance, while those with smaller *kl/r* and larger *b/t* showed the worst. Local buckling precipitates low cycle fatigue causing lower ductility capacity for the built-up braces with smaller *kl/r* and larger *b/t*; however, for those with larger *kl/r*, ductility capacity was not much affected by the *b/t* ratio. The BLMs with section shape "A" (forming I shapes) exhibited more ductile behavior than those with section shape "B" (forming box shapes), because lacing buckling of section shape "B" BLMs worsened the strength degradation in compression. Overall, BLMs with larger slenderness ratio were shown to have less ductility capacity than monolithic bracing members (Lee and Bruneau, 2002, 2005), while those with smaller slenderness ratio showed ductility capacity comparable to monolithic bracing members.

The BLMs designed with larger *kl/r* and smaller *b/t* were observed to dissipate larger normalized cumulative energy than those designed with smaller *kl/r* and larger *b/t*; this is a similar trend to what was observed for monolithic braces by Lee and Bruneau (2002, 2005). On average, the tested BLMs with section shape "B" dissipated less normalized cumulative energy than monolithic bracing members, however those with section shape "A" dissipated slightly more normalized cumulative energy.

The normalized compressive strength degradation, C_r''/C_r of BLMs typically decrease as normalized displacements $\delta/\delta_{b,exp}$ increase, and the ratios for specimens with larger slenderness ratio dropped more rapidly than those with smaller slenderness ratio; similar trends were observed for the monolithic braces (Lee and Bruneau, 2002, 2005).

The BLMs with smaller slenderness ratio, *kl/r*, and width-to-thickness ratio, *b/t*, experienced a larger number of inelastic cycles than those with larger slenderness ratio and width-to-thickness ratio. The low cycle fracture life criteria proposed by other researchers, Tang and Goel (1987) and Archambault *et al*. (1995), either over- or under-estimated the fracture life of the BLMs. A new criterion was proposed in this study that is applicable for estimating the low cycle fracture life of the BLMs, which is safer than Archambault's *et al*. model and less conservative than Tang and Goel's model.

Acknowledgements

This work was conducted at the University at Buffalo and was supported by the Federal Highway Administration under contract number DTFH61-98-C-00094 to the Multidisciplinary Center for Earthquake Engineering Research. However, any opinions, findings, conclusions, and recommendations presented in this paper are those of the authors and do not necessarily reflect the views of the sponsors.

References

American Institute of Steel Constructions, Inc. (1999), "Load and Resistance Factor Design Specification for Structural Steel Buildings," AISC, Chicago, Illinois.

Archambault Marie-Hélène, Tremblay, R and Filiatrault A (1995), "Étude du Comportment Séismique des Contreventements Ductiles en X Avec Profilés Tubulaires en Acier," *Rapport No. EPM/GCS-1995-09*, Département de Génie Civil Section Structures, École Polytechnique, Montréal, Quebec, Canada.

Gere JM and Timoshenko SP (1984), *Mechanics of Material*, Brooks/Cole Engineering Division, Wadsworth, Inc., Belmont, California.

Lee K and Bruneau M (2002), "Review of Energy Dissipation of Compression Members in Concentrically Braced Frames," *Report No. MCEER-02-0005*, October, Multidisciplinary Center for Earthquake Engineering Research, State University of New York, Buffalo, New York.

Lee K and Bruneau M (2004), "Seismic Vulnerability Evaluation of Axially Loaded Steel Built-up Laced Members," *Report No. MCEER-04-0007*, June, Multidisciplinary Center for Earthquake Engineering Research, State University of New York, Buffalo, New York.

Lee K and Bruneau M (2005), "Energy Dissipation of Compression Members in Concentrically Braced Frames: Review of Experimental Data," *Journal of Structural Engineering*, ASCE, **131**(4): 552-559.

Lee K and Bruneau M (2008), "Seismic Vulnerability Evaluation of Axially Loaded Steel Built-up Laced members I: Experimental Results," *Earthquake Engineering and Engineering Vibration*, **7**(2): 113-124.

Lee S and Goel SC (1987), "Seismic Behavior of Hollow and Concrete-Filled Square Tubular Bracing Members," *Report No. UMEE 87-11*, December, Department of Civil Engineering, The University of Michigan, Ann Arbor, Michigan.

Tang XD and Goel SC (1987), "Seismic Analysis and Design Considerations of Braced Steel Structures," *Report No. UMCE 87-4*, April, Department of Civil Engineering, The University of Michigan, Ann Arbor, Michigan.